doi:10.1093/brain/awz371 BRAIN 2020: 143; 359–373 | 359

BRAIN
A JOURNAL OF NEUROLOGY

Regional differences in Alzheimer's disease pathology confound behavioural rescue after amyloid-β attenuation

Christopher D. Morrone,[1,2] Paolo Bazzigaluppi,[3] Tina L. Beckett,[1] Mary E. Hill,[1] Margaret M. Koletar,[3] Bojana Stefanovic[3,4] and JoAnne McLaurin[1,2]

Failure of Alzheimer's disease clinical trials to improve or stabilize cognition has led to the need for a better understanding of the driving forces behind cognitive decline in the presence of active disease processes. To dissect contributions of individual pathologies to cognitive function, we used the TgF344-AD rat model, which recapitulates the salient hallmarks of Alzheimer's disease pathology observed in patient populations (amyloid, tau inclusions, frank neuronal loss, and cognitive deficits). *scyllo*-Inositol treatment attenuated amyloid-β peptide in disease-bearing TgF344-AD rats, which rescued pattern separation in the novel object recognition task and executive function in the reversal learning phase of the Barnes maze. Interestingly, neither activities of daily living in the burrowing task nor spatial memory in the Barnes maze were rescued by attenuating amyloid-β peptide. To understand the pathological correlates leading to behavioural rescue, we examined the neuropathology and *in vivo* electrophysiological signature of the hippocampus. Amyloid-β peptide attenuation reduced hippocampal tau pathology and rescued adult hippocampal neurogenesis and neuronal function, via improvements in cross-frequency coupling between theta and gamma bands. To investigate mechanisms underlying the persistence of spatial memory deficits, we next examined neuropathology in the entorhinal cortex, a region whose input to the hippocampus is required for spatial memory. Reduction of amyloid-β peptide in the entorhinal cortex had no effect on entorhinal tau pathology or entorhinal-hippocampal neuronal network dysfunction, as measured by an impairment in hippocampal response to entorhinal stimulation. Thus, rescue or not of cognitive function is dependent on regional differences of amyloid-β, tau and neuronal network dysfunction, demonstrating the importance of staging disease in patients prior to enrolment in clinical trials. These results further emphasize the need for combination therapeutic approaches across disease progression.

1 Sunnybrook Research Institute, Biological Sciences, 2075 Bayview Ave, Toronto, ON M4N 3M5, Canada
2 University of Toronto, Faculty of Medicine, Department of Laboratory Medicine and Pathobiology, 1 King's College Cir, Toronto, ON M5S 1A8, Canada
3 Sunnybrook Research Institute, Physical Sciences, 2075 Bayview Ave, Toronto, ON M4N 3M5, Canada
4 University of Toronto, Faculty of Medicine, Department of Medical Biophysics, 101 College St Suite 15-701, Toronto, ON M5G 1L7, Canada

Correspondence to: Christopher Morrone
Sunnybrook Research Institute
2075 Bayview Ave, S1-19
M4N 3M5, Toronto, ON, Canada
E-mail: chris.morrone@mail.utoronto.ca

Keywords: Alzheimer's disease; cognition; hippocampal-entorhinal circuitry; tau; amyloid-β

Abbreviation: NTg = non-transgenic

Received May 14, 2019. Revised September 16, 2019. Accepted October 1, 2019. Advance Access publication November 28, 2019

Introduction

Alzheimer's disease is the most common cause of dementia and is defined neuropathologically by the presence of amyloid-β plaques and neurofibrillary tangles (NFTs) of hyperphosphorylated tau (Selkoe and Hardy, 2016). Much controversy surrounds the contribution of various pathologies to memory loss, which appears to associate more strongly with neurodegeneration and tau pathology in patients than it does with amyloid-β pathology (Selkoe and Hardy, 2016; Franzmeier *et al.*, 2019; Gordon *et al.*, 2019). A large portion of research has focused on amyloid-β driven rodent models lacking critical hallmarks of Alzheimer's disease (NFTs, neuronal death), which confounds the ability to ascertain relative contributions of different pathologies to cognitive compromise.

Hippocampal dysfunction has long been thought to drive memory impairments in Alzheimer's disease. Recently this focus has shifted to include the entorhinal cortex, a region that provides excitatory input into the hippocampal trisynaptic circuit, and is affected early in Alzheimer's disease progression (Braak and Braak, 1991; Anacker and Hen, 2017). Overexpression of mutated human tau (P301L) in mouse models results in neuronal silencing and loss of excitatory neurons in entorhinal cortex, leading to spatial memory deficits and tau propagation (Fu *et al.*, 2017, 2019; Busche *et al.*, 2019). Evidence from tau PET and diffusion tensor imaging suggest that tau pathology spreads along functional connections propagating neurodegeneration in humans (Jacobs *et al.*, 2018).

The hippocampus regulates behavioural responses to a changing environment through circuit modulatory effects of newborn neurons generated through adult hippocampal neurogenesis. These behaviours include pattern separation and executive function as assessed by cognitive flexibility in reversal learning (Lepousez *et al.*, 2015; Anacker and Hen, 2017). Pattern separation involves the disambiguation between learned stimuli and novel stimuli into distinct neuronal networks, whereas executive functions consist of multiple high-level cognitive processes that drive rule generation and behavioural selection. These processes are essential to normal human behaviour, and are disrupted in Alzheimer's disease and Alzheimer's disease models (Lepousez *et al.*, 2015; Morrone *et al.*, 2016; Toda *et al.*, 2018; Moreno-Jiménez *et al.*, 2019).

TgF344-AD rats overexpress human amyloid precursor protein with the Swedish mutation (KM670/671NL; APPswe) and presenilin with exon 9 excised (PS1ΔE9), which drive human amyloid-β production, followed by hyperphosphorylated tau inclusions, neuronal loss and cognitive deficits (Cohen *et al.*, 2013). At 6 months of age, TgF344-AD rats begin to accumulate cortical and hippocampal amyloid-β and exhibit deficits in hippocampal-dependent synaptic circuits (Cohen *et al.*, 2013; Muñoz-Moreno *et al.*, 2018; Stoiljkovic *et al.*, 2019), with hyperphosphorylation of tau, and tau+ inclusions primarily in the locus coeruleus (Cohen *et al.*, 2013; Rorabaugh *et al.*, 2017). By 9 months of age, there is an approximate 40% loss of CA1 GABAergic cells and hippocampal neuronal dysfunction, progressing to ∼39% loss of hippocampal neurons, cortical and hippocampal NFTs and significant behavioural impairment by 16 months of age (Cohen *et al.*, 2013; Rorabaugh *et al.*, 2017; Bazzigaluppi *et al.*, 2018; Voorhees *et al.*, 2019). Thus, we examined the contribution of combined pathologies to cognitive function, and the effect of amyloid-β attenuation in disease-bearing TgF344-AD rats. To attenuate amyloid-β, *scyllo*-inositol treatment was chosen because it is orally available and actively transported into the brain where it directly binds amyloid-β, reducing amyloid-β aggregates and amyloid plaques by the promotion of *scyllo*-inositol-amyloid-β clearance (McLaurin *et al.*, 2006; Hawkes *et al.*, 2012; reviewed in Ma *et al.*, 2012).

Materials and methods

Animal care and treatment

TgF344-AD rats overexpress human APPswe and PS1ΔE9, under the control of the mouse prion promotor, outbred on a Fischer 344 rat background. All animal procedures were approved by the Animal Care Committee of the Sunnybrook Research Institute (#19-655), and in accordance with the ethical standards of the Canadian Council on Animal Care guidelines. Rats were bred in-house and kept on a 12-h light-dark cycle with *ad libitum* access to chow and water. Sex-balanced and aged-matched TgF344-AD and non-transgenic (NTg) littermate rats were randomly divided into treatment and non-treatment groups. *scyllo*-Inositol (SI) (kind gift from Transition Therapeutics Inc), was administered *ad libitum* at 10 mg/ml in drinking water as per Fenili *et al.* (2007). Treatment began at 9 months of age and continued until sacrifice at 13 months.

One group of rats (cohorts: NTg, NTg-SI, Tg, Tg-SI; n = 32) received injections of the thymidine analogues 5-bromo-2′-deoxyuridine (BrdU) (Sigma-Aldrich) and 5-ethynyl-2′-deoxyuridine (EdU) (Sigma-Aldrich), which incorporate into the DNA of replicating cells. Each rat was administered five daily intraperitoneal injections of 50 mg/kg BrdU (3–4 weeks prior to sacrifice) and of 50 mg/kg EdU (1–5 days prior to sacrifice) to label hippocampal cell survival and proliferation, respectively. Six hours following the last EdU injection, under anaesthesia with isoflurane (5% induction and 2% maintenance), rats were transcardially perfused with phosphate-buffered saline (PBS) followed by 4% paraformaldyhyde (pH 7.4). An additional group (cohorts: NTg, NTg-SI, Tg, Tg-SI; n = 64) were tested on behavioural tasks between 12 and 13 months of age (in order: burrowing, open field, novel object recognition and Barnes maze). A third group of rats (cohorts: NTg, Tg, Tg-SI; n = 22) were assessed by *in vivo* electrophysiology. The exact number of rats per cohort and experiment are indicated in the figure legends.

Behavioural testing

Burrowing

Burrowing was used to measure activities of daily living (Deacon, 2009). Rats were habituated to the burrowing cage and tube with cage mates for 30 min and were tested alone for 2 h on the same day. For the habituation period the tube was filled with bedding material 20 cm from the top. For the testing period the tube was filled 5 cm from the top. The amount of bedding in the tube was weighed before and after testing. The per cent material removed from the tube was quantified.

Open field and novel object recognition

All tasks were conducted in a behavioural suite. Trials were filmed, collected and analysed using EthoVision XT (11.5). Rats were placed in the centre of a black open field (100 cm × 100 cm, 30 cm walls), and allowed to explore for 10 min (used for open field analyses). Following a 3-h delay, there was another 10-min habituation to acclimatize the rats to the novel object recognition field. On the next day, a 5-min habituation was conducted (no objects). An hour later a 5-min object familiarization phase was conducted (two of Object A). An hour later a 5-min testing period was conducted (one of Object A and Object B). Objects were randomly assigned as A and B (Duplo® tower, or cell culture flask filled with bedding). Object recognition times were scored manually by a blinded investigator and the novel object recognition ratio was calculated by the following [(time novel object)/(time novel object + time familiar object)]. Object exploration was defined when a rat directed its nose at an object within ~2 cm or less, and was actively investigating the object.

Barnes maze

The Barnes maze task was conducted in the same behavioural suite with spatial cues. Trials were filmed, collected and analysed using EthoVision. A circular field (Maze Engineers) was used (20 holes, one is the escape box). Rats were trained to the location of the escape box. Each day of testing involved two 3-min trials with an aversive overhead light. For 3 days, rats were tested on finding the escape box. After 3 days rest, rats were probed for recall of the escape box location. Immediately following the probe, 5 days of reversal testing was conducted in which the escape box was switched to the opposite side of the maze. Trials were analysed for latency to escape. Search strategies were manually scored by a blinded investigator and given numerical values for statistical analyses: direct (1), corrected (0.75), long correction (0.5), focused search (0.5), serial (0.25), and random (0) (Illouz *et al.*, 2016).

Immunofluorescence and immunohistochemistry

Forty-micrometre sections were collected throughout the rat hippocampus and entorhinal cortex (bregma –1.80 mm through –8.00 mm) with a sliding microtome, Microm HM400. Hippocampal and entorhinal cortical amyloid-β plaque load were assessed as previously reported (McLaurin *et al.*, 2006). One in every 20 hippocampal sections were sampled, starting from bregma –2.28, and one in every 10 entorhinal cortical sections were sampled, starting from bregma –5.64. To assess neurogenesis proliferation and survival, double immunofluorescent staining and cell counts of EdU co-localized with doublecortin (DCX), and of BrdU co-localized with neuronal nuclei (NeuN) were conducted, respectively (Supplementary material). One in every 10 hippocampal sections were sampled, starting from Bregma –2.28 mm, as previously reported (Morrone *et al.*, 2016). Double staining immunofluorescence of tau with amyloid-β plaques was conducted to demonstrate interaction. For tau immunohistochemistry, one in every 20 hippocampal sections were sampled, starting from bregma –3.08, and one in every 10 entorhinal cortical sections were sampled, starting from bregma –5.64, as previously described (d'Abramo *et al.*, 2013). Details for all primary and secondary antibodies/detection reagents are provided in Supplementary Table 1. Immunofluorescence was imaged on a Nikon A1 laser scanning confocal microscope. Immunohistochemistry was imaged on a Zeiss Observer Z1 microscope. Tissue analyses were conducted in ImageJ.

Plasma amyloid-β ELISAs

Amyloid-β_{40} (Invitrogen; KHB3481) and amyloid-β_{42} (Invitrogen; KHB3441) ELISAs were conducted following the manufacturer's guidelines. Amyloid-β_{40} and amyloid-β_{42} concentrations (pg/ml) were determined by fitting the standard curve. All samples and standards were run in triplicate.

Electrophysiology

Animals were anaesthetized with isofluorane (5% induction, 1–1.5% maintenance) and positioned in a stereotaxic frame (David KOPF Instruments). A cranial window was inserted over the right hemisphere extending from bregma to lambda (Bazzigaluppi *et al.*, 2018). Two double-shank linear multielectrode arrays were used (Supplementary Fig. 1): the first was lowered into the right dorsal hippocampus (AP –3.0 mm from bregma, ML ± 2.5 mm, depth 4 mm), and the second into the right medial entorhinal cortex [4° angle in the lateral direction, AP +2.0 mm from transverse sinus (approximately –9.5 to –10.0 mm from bregma), ML ± 3.5 mm, depth 7.0 mm]. Local field potentials were pre-amplified by the stimulating and recording head-stage (Product 962000) and then amplified (A-M systems 3600) between 0.3 Hz and 5 kHz, sampled at 20 kHz (DataWave). For intracranial entorhinal cortex stimulation, the stimulator was connected to the caudal linear multi-electrode array to deliver a single 5 μs pulse at 500 mV and 1000 mV through the two deepest electrodes in the entorhinal cortex (Supplementary Fig. 2). Stimulation was repeated 15 times per amplitude step every 5–6 s. Raw recordings and analysis scripts are available from the authors on request. Analysis was conducted in MATLAB (MathWorks) and adapted from previous work (Pettersen *et al.*, 2006; Tort *et al.*, 2009; Canolty and Knight, 2010; Bazzigaluppi *et al.*, 2018). Additional details for all experimental procedures are provided in the Supplementary material.

Statistical analysis

For pathological and electrophysiological assessments, we based our sample size on previous experience and published work (McLaurin *et al.*, 2006; Morrone *et al.*, 2016; Bazzigaluppi *et al.*, 2018). In light of up to 20% variation in

behavioural readouts, and ensuring power of at least 80% across all contrasts, we thus required 16 rats per group at a significance level of 5% for behavioural analyses to reach statistical significance. Data were excluded from the novel object recognition dataset: 18 rats spread across all four cohorts were excluded from analysis for task non-performance (i.e. not investigating the objects in the test phase). No other data exclusions were made, nor were outliers removed. Investigators were blinded to genotype and treatment during data collection and data analysis. Rats were identified by number and grouped into cohorts after all data were collected and analysed, prior to statistical analysis.

GraphPad Prism 6 (GraphPad Software, Inc.), SPSS (IBM, version 23) or R were used for statistical analyses and generation of graphs. One-way ANOVA with a Holm-Sidak *post hoc* test was used for multiple comparisons (pathology and behaviour analyses with four groups). Linear regression and repeated measures ANOVA with a Holm-Sidak *post hoc* test were conducted for Barnes maze learning and reversal learning analyses. Unpaired *t*-test was used for pathological comparisons involving two groups. For electrophysiology analyses a one-way ANOVA with a paired *t*-test with false discovery rate correction (cross-frequency coupling) or a Kruskal-Wallis H test followed by Wilcoxon signed-rank test with false discovery rate correction (stimulation) were conducted. All data were analysed as two-sided and presented as the mean ± standard error of the mean (SEM) or mean ± 95% confidence interval (CI) for slope values.

Data availability

Data are reported within the text, figures and Supplementary material. Raw data are available upon request.

Results

To model amyloid-β lowering strategies, we used *scyllo*-inositol to reduce amyloid-β burden. We have previously demonstrated that *scyllo*-inositol reduces both parenchymal and vascular amyloid-β in an APP overexpressing mouse model (McLaurin *et al.*, 2006; Dorr *et al.*, 2012). Sex-balanced groups of 9-month-old TgF344-AD rats and NTg littermates were treated or untreated with *scyllo*-inositol for 4 months before undergoing cognitive, pathological and neuronal network characterization.

Partial rescue of behavioural tasks from amyloid-β attenuation

We used a battery of tasks to probe behaviours including activities of daily living and cognitive function. All animals were tested on the burrowing task, to measure an activity of daily living, open field task to determine anxiety and baseline activity, novel object recognition to probe place discrimination, and Barnes maze to examine learning, spatial memory and executive function. These tasks were chosen to probe behaviour across the spectrum of disease as well as to probe the role of various brain regions in cognitive dysfunction and rescue in disease-bearing TgF344-AD rats. There was an overall effect of genotype and treatment on burrowing behaviour [$F(3,60) = 20.72$, $P < 0.0001$; Fig. 1A]. TgF344-AD rats display a significant deficit compared to NTg rats ($P = 0.001$); however, there was no effect of amyloid-β attenuation in TgF344-AD rats ($P = 0.37$). Deficits in activities of daily living were not due to differences in activity or anxiety as no overall differences were observed in percentage of time spent in the centre of the open field [$F(3,60) = 2.12$, $P = 0.11$] nor distance moved during the task [$F(3,60) = 0.80$, $P = 0.50$; Supplementary Fig. 3]. To probe place discrimination, novel object recognition performance was determined by differential time spent with a novel versus a familiar object. Novel object recognition involves the recollection of familiar stimuli, and the disambiguation between familiar and novel stimuli. This confers both recognition memory function, which is regulated by hippocampal and perirhinal cortical signalling (Squire *et al.*, 2007), and pattern separation, which is regulated by hippocampal neurogenesis (Jessberger *et al.*, 2009; Lepousez *et al.*, 2015). An overall effect on the novel object recognition task [$F(3,42) = 7.36$, $P = 0.0004$; Fig. 1B] , showed TgF344-AD rats have a deficit in recognizing the novel object when compared to NTg rats ($P = 0.04$). Amyloid-β attenuation rescues pattern separation in TgF344-AD rats ($P = 0.002$), with no effect of treatment in NTg rats ($P = 0.34$). A rescue in place discrimination but not activities of daily living, suggests an improvement in hippocampal function in TgF344-AD rats.

To probe hippocampal function further, rats were tested for learning, spatial memory and reversal learning in the Barnes maze task, which is dependent on the ability of the rat to learn and remember an escape from an aversive environment. There were no significant differences in learning between all cohorts [$F(3,60) = 0.62$, $P = 0.60$]. Rats were tested for long-term spatial memory in a probe trial, which showed no overall differences in the latency to escape [($F(3,60) = 1.77$, $P = 0.16$; Fig. 1C]. To determine the level of cognitive resources used to complete this task, evaluation of search strategy complexity was used (Illouz *et al.*, 2016). There was an effect of genotype and treatment on search strategy complexity used in probe trials [$F(3,60) = 5.73$, $P = 0.002$; Fig. 1D]. TgF344-AD rats used significantly weaker search strategies than untreated NTg rats ($P = 0.008$) and no effect of amyloid-β attenuation was observed in TgF344-AD rats ($P = 0.68$). These data demonstrate that TgF344-AD rats are deficient in spatial memory recall, even after treatment.

To probe executive function, rats underwent reversal learning in the Barnes maze, a task requiring cognitive flexibility. There was an overall effect on the latency to escape in the Barnes maze reversal learning phase [$F(3,60) = 4.61$, $P = 0.006$; Fig. 1E]. Linear regression, across the 10 trials, demonstrated a strong improvement in all groups except untreated TgF344-AD rats. In the final trial, TgF344-AD rats were significantly slower to escape than NTg rats ($P = 0.0001$), and amyloid-β

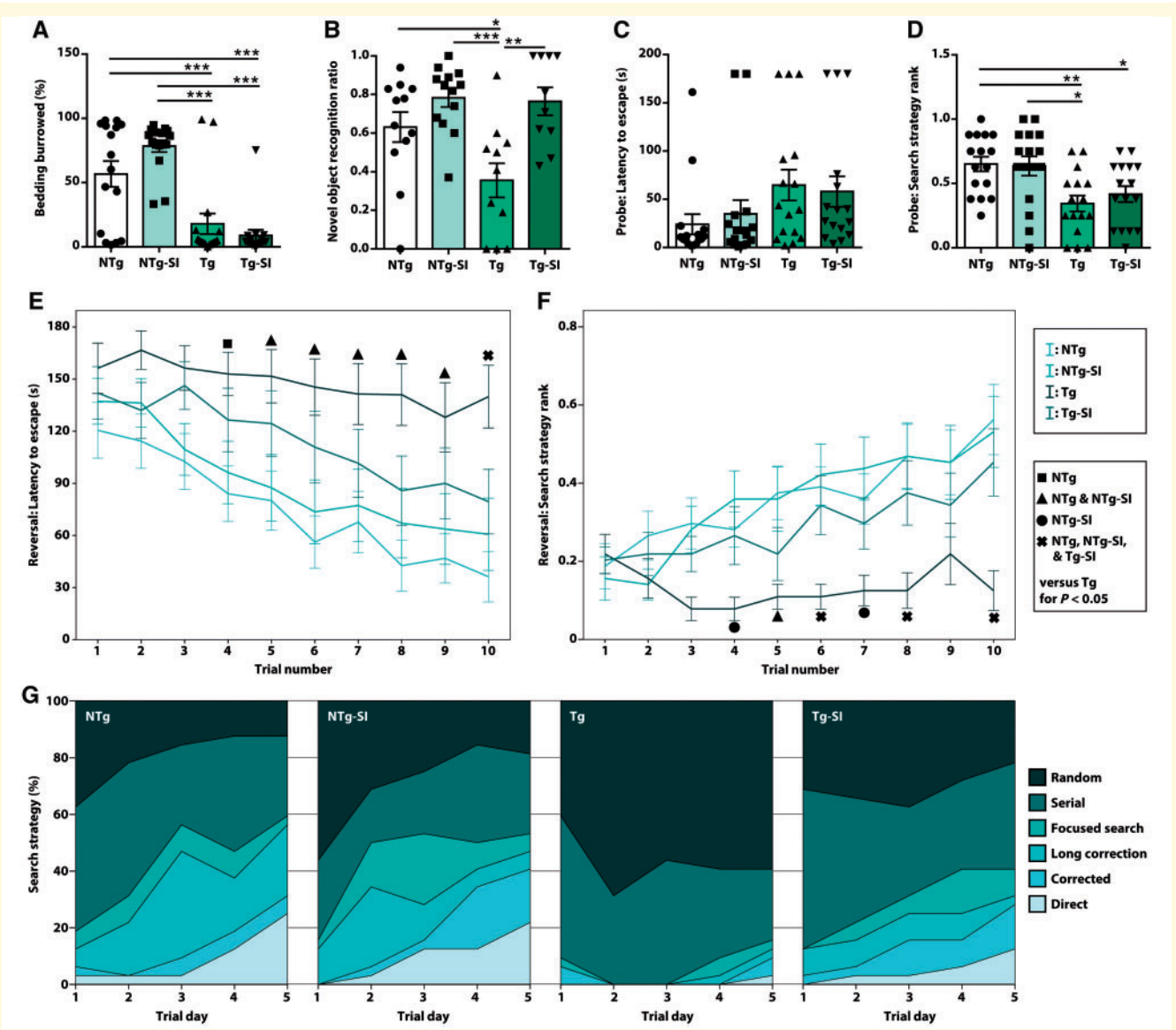

Figure 1 Amyloid-β attenuation rescues pattern separation and executive function but not activities of daily living and spatial memory. Tg and NTg rats untreated or treated to attenuate amyloid-β (Tg-SI, NTg-SI), were tested on a battery of behavioural tasks. (**A**) TgF344-AD rats exhibit deficits in the burrowing task that were not rescued by treatment (n = 16). (**B**) TgF344-AD rats have impaired pattern separation in the novel object recognition task, which was rescued by amyloid attenuation (from n = 16, rats were excluded for not performing the task: NTg = 12; NTg-SI = 13; Tg = 11; Tg-SI = 10). (**C** and **D**) TgF344-AD rats, regardless of treatment, exhibit a trend to deficits in latency to escape and significant deficits in search strategies used in the Barnes maze spatial memory probe (n = 16). (**E**) Reversal learning phase demonstrated NTg (–9.72 ± 1.70), NTg-SI (–8.97 ± 1.96) and Tg-SI (–7.56 ± 1.97) rats decreased escape latency across 10 trials, whereas Tg rats (–3.24 ± 1.70) did not (n = 16). (**F** and **G**) Search strategies utilized by the NTg, NTg-SI and Tg-SI rats significantly improved, whereas Tg rats did not improve (n = 16). Mean ± standard error of mean (SEM) or 95% confidence interval (CI) (linear regression), one-way (**A**–**D**) or repeated measures (**E** and **F**) ANOVA with Holm-Sidak *post hoc* test, $^{*}P < 0.05$; $^{**}P < 0.01$; $^{***}P < 0.001$.

attenuation rescued this deficit in TgF344-AD rats (P = 0.05; Fig. 1E). There was an overall effect of genotype and treatment on search strategy complexity across the reversal phase [$F(3,60)$ = 5.69, P = 0.002; Fig. 1F]. NTg, NTg-SI and Tg-SI rats utilized a high percentage of direct search strategies in later trials, while untreated TgF344-AD rats used mostly indirect search strategies across all trials (Fig. 1G) (Illouz *et al.*, 2016). In the final trial, TgF344-AD rats used significantly weaker search strategies than NTg rats ($P < 0.0001$). Amyloid-β attenuation rescued this deficit in TgF344-AD rats (P = 0.002; Fig 1F). Overall, these data indicate a strong deficit in reversal learning and executive function in TgF344-AD rats, and improvements of these behaviours from amyloid-β attenuation.

scyllo-Inositol treatment was shown to decrease amyloid-β pathology brain-wide in mouse models of Alzheimer's

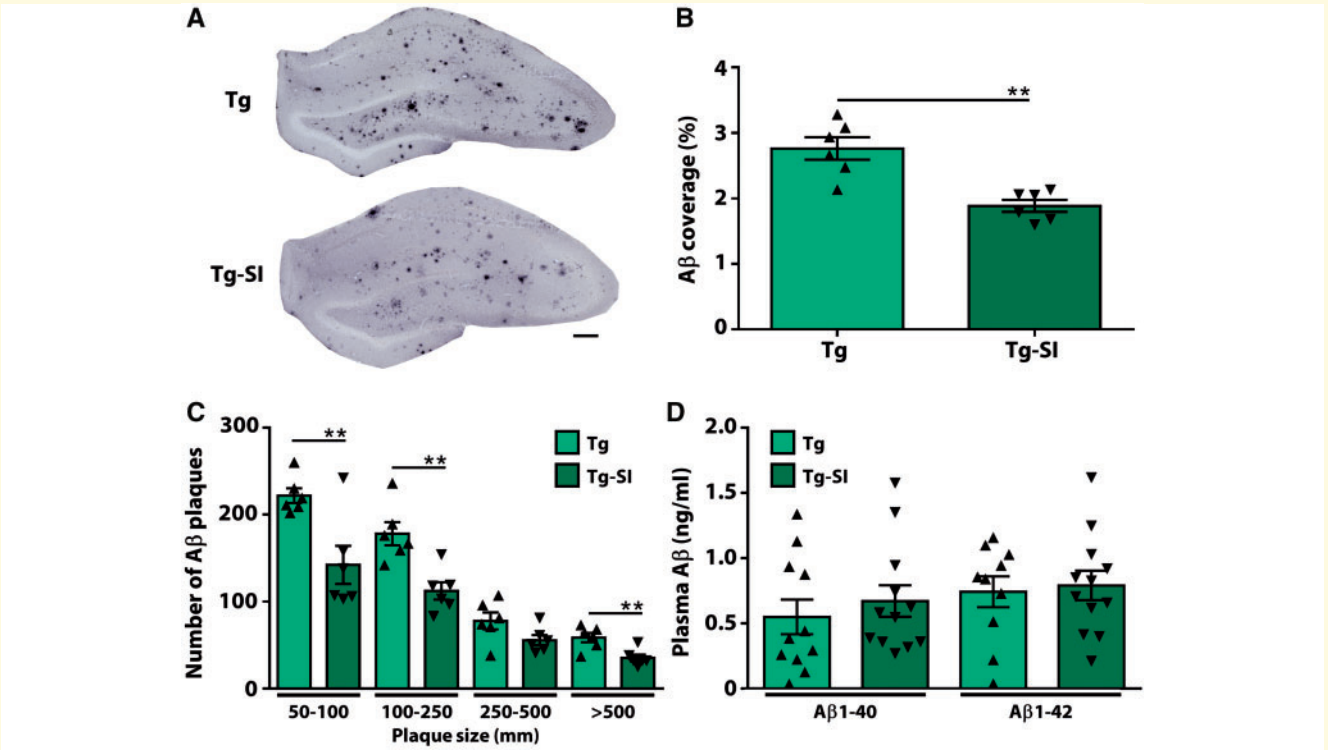

Figure 2 Therapeutic administration of *scyllo*-inositol reduced amyloid-β load. (**A**) Tg-SI rats visually demonstrate decreased amyloid-β coverage and plaque size in the hippocampus. Scale bar = 100 μm. (**B**) The percentage of hippocampal area covered by amyloid-β plaques is significantly attenuated in Tg-SI, and (**C**) plaques of all sizes are reduced. (**D**) Levels of plasma amyloid-$\beta_{40/42}$ are unchanged indicating that clearance pathways are maintained. n = 6 per group (**B** and **C**) and n = 10–12 per group (**D**): amyloid-β_{40} Tg: n = 11; amyloid-β_{42} Tg: n = 10; amyloid-$\beta_{40/42}$ Tg-SI n = 12 (mean ± SEM, two-sided unpaired t-test, $^{**}P < 0.01$).

disease (McLaurin *et al.*, 2006; Fenili *et al.*, 2007; Morrone *et al.*, 2016). To evaluate the efficacy in TgF344-AD rats, we quantified hippocampal amyloid-β pathology (Fig. 2). Treatment significantly decreased amyloid-β plaque coverage in the hippocampus (P = 0.001; Fig. 2A and B) and decreased numbers of plaques of all sizes by 35.6 ± 9.5% (Fig. 2C). To determine amyloid-β clearance pathways, we assessed plasma amyloid-β_{40} and amyloid-β_{42} in TgF344-AD rats treated and untreated with *scyllo*-inositol and detected no differences (P = 0.51 and P = 0.77, respectively) (Fig. 2D). In agreement with our previous studies, *scyllo*-inositol did not alter peripheral clearance pathways and clearance of amyloid-β by microglial cells (Supplementary Fig. 4) (McLaurin *et al.*, 2006; Hawkes *et al.*, 2012). Overall these data confirm *scyllo*-inositol-induced amyloid-β attenuation.

Contribution of hippocampal neurogenesis to the rescue of behavioural deficits

To investigate mechanisms leading to behavioural rescue, we assessed TgF344-AD rats for measures of adult hippocampal neurogenesis. Progenitor cells in the subgranular zone of the dentate gyrus self-renew or generate astrocytic or neuronal lineage cells; the latter contribute to learning and memory tasks via integration into the hippocampal circuit and thus we focused on this population (Lepousez *et al.*, 2015; Anacker and Hen, 2017). TgF344-AD and NTg rats, treated or untreated with *scyllo*-inositol, were phenotyped for hippocampal proliferating and surviving cells within a neuronal lineage (Fig. 3). An overall effect of genotype and treatment was detected on total proliferating neural progenitor cells in the dentate gyrus [$F(3,26)$ = 9.34, P = 0.0002; Fig. 3A]. TgF344-AD rats exhibit an increased number of proliferating cells compared to NTg rats (P = 0.002); however, *scyllo*-inositol treatment had no effect (P = 0.95). Of the proliferating cell population, an overall effect on percentage of newborn neurons and on total number was detected [$F(3,26)$ = 11.90, $P < 0.0001$; Fig. 3B; $F(3,26)$ = 3.14, P = 0.04, respectively]. TgF344-AD rats have significantly fewer hippocampal proliferating cells expressing a neuronal phenotype than NTg rats, which was rescued by amyloid-β attenuation (P = 0.0001 and P = 0.006, respectively) (Fig. 3B). There was no effect of *scyllo*-inositol in NTg rats (P = 0.81). Overall these data demonstrate that TgF344-AD rats exhibit increased neural progenitor cell proliferation, of which fewer are differentiating into a neuronal phenotype. With *scyllo*-inositol treatment, deficits in neuronal differentiation

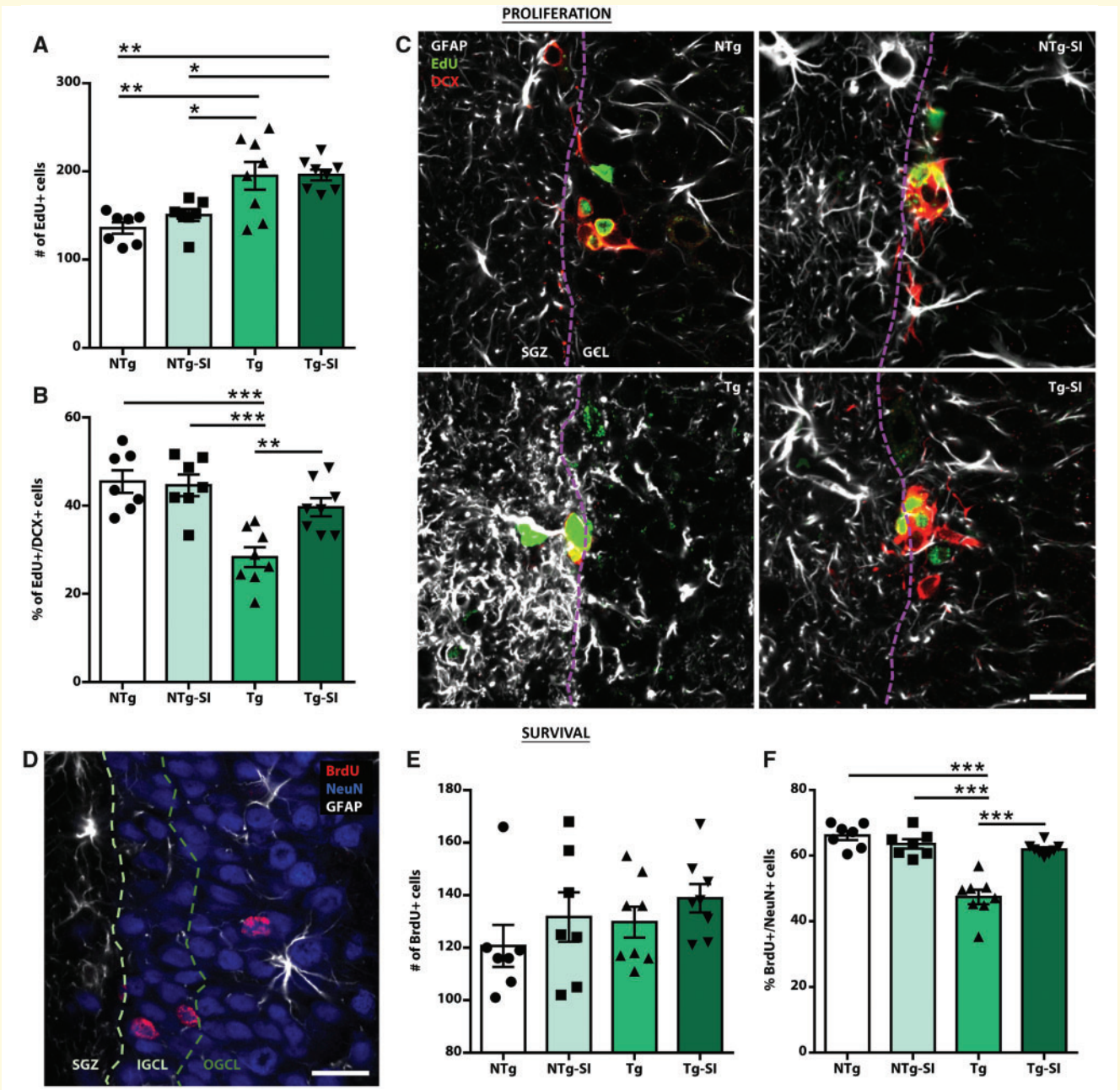

Figure 3 Deficits in differentiation and survival of newborn neurons rescued by amyloid-β attenuation. Untreated and treated NTg and TgF344-AD rats were injected with EdU and BrdU to label proliferating and surviving cells, respectively. (**A**) Tg rats, regardless of treatment, exhibit a significant increase in EdU+ proliferating cells. (**B**) However, Tg rats have significantly fewer newborn cells expressing a neuronal phenotype (EdU+ DCX+). This deficit is rescued in Tg-SI rats. (**C**) GFAP (white), EdU (green), and DCX (red) labelling in the subgranular zone (SGZ) and granule cell layer (GCL) of NTg, NTg-SI, Tg and Tg-SI rats, demonstrate deficits in neuronal differentiation and migration in Tg rats, which were rescued in Tg-SI rats. (**D**) BrdU (red), NeuN (blue) and GFAP (white) staining demonstrate the integration of surviving newborn neurons into the granule cell layer. (**E**) No genotype or treatment differences were detected in number of BrdU+ surviving cells. (**F**) Tg rats exhibit significant deficits in survival of newborn neurons, (BrdU+ NeuN+), which were rescued by treatment. (**C** and **D**) Dashed lines separate subgranular zone and inner and outer granule cell layers. Scale bars = 20 μm. NTg and NTg-SI n = 7; Tg and Tg-SI n = 8 (mean ± SEM, one-way ANOVA with Holm-Sidak *post hoc* test, $^{*}P < 0.05$; $^{**}P < 0.01$; $^{***}P < 0.001$).

are attenuated, while maintaining increased proliferation (Fig. 3C), suggesting that hippocampal neurogenesis may be compensating for pathology-related hippocampal deficits.

To quantify and phenotype survival of newborn neurons, neuronal maturation was examined (Fig. 3D). Although no overall effect was detected on the total number of surviving cells in the dentate gyrus [$F(3,26) = 1.08$, $P = 0.37$;

Fig. 3E], there was an effect on the percentage and number of surviving newborn neurons [$F(3,26) = 30.95$, $P < 0.0001$; Fig. 3F; $F(3,26) = 5.28$, $P = 0.006$, respectively]. TgF344-AD rats have a significantly lower percentage of and fewer total surviving neurons than NTg rats ($P < 0.0001$, $P = 0.05$); both were rescued by amyloid-β attenuation ($P < 0.0001$; $P = 0.008$). Integration of newborn neurons into the inner and outer granule cell layer facilitates their maturation and functional signalling through hippocampal synaptic circuits (Lepousez *et al.*, 2015; Toda *et al.*, 2018). Newborn neurons in TgF344-AD rats were deficient in migration and these deficits were reversed by amyloid-β attenuation (Supplementary Fig. 5). Overall these data demonstrate that removal of amyloid-β in TgF344-AD rats rescued deficits in differentiation, migration and survival of newborn neurons in the hippocampus.

Hippocampal neuronal integrity and functional rescue contributes to cognitive benefit

We have previously reported loss of hippocampal neurons in 9-month-old TgF344-AD rats; this loss led to attenuation of phase amplitude coupling within hippocampal neuronal networks in comparison with NTg littermates (Bazzigaluppi *et al.*, 2018). Thus, we quantified neuronal density in the hippocampus of TgF344-AD rats. We compared the densities of neuronal staining in the granule cell layer, normalized to hippocampal area, and observed a stark deficit in TgF344-AD rats (Fig. 4A). There was an overall effect of genotype and treatment on neuronal density [$F(3,28) = 5.05$, $P = 0.006$; Fig. 4B]. TgF344-AD rats have a significant loss (11 ± 3.6%) in neuronal integrity, compared to NTg rats ($P = 0.02$), which was rescued by amyloid-β attenuation ($P = 0.02$). Although we cannot distinguish whether neuronal integrity was a function of rescued neurogenesis, inhibition of amyloid-β-driven neuronal loss or a combination of these two mechanisms, these data support the hypothesis that rescue of hippocampal neuronal integrity contributes to behavioural improvements.

Impaired cognitive function in both humans and rodents is related to temporal modulation of theta oscillations and theta-gamma coupling (Bott *et al.*, 2016). A sensitive predictor of cognitive function is coupling between the phase of a slow oscillation (i.e. theta) and the amplitude of a faster oscillation (i.e. gamma) because of its role in information processing (Tort *et al.*, 2009; Canolty and Knight, 2010). To determine whether neuronal rescue had functional correlates, we assessed hippocampal neuronal network function in untreated and treated TgF344-AD rats in comparison to NTg rats using *in vivo* electrophysiological recordings to measure cross-frequency coupling. An overall effect of genotype and treatment was detected on hippocampal modulation index in theta low-gamma and theta high-gamma bands [$F(2,40191) = 113.00$, $P < 0.0001$; $F(2,81771) = 160.30$, $P < 0.0001$, respectively; Fig. 4C]. When compared to NTg rats, TgF344-AD rats exhibit deficits between theta low-gamma and between theta high-gamma bands, which are partly reversed by amyloid-β attenuation (all $P < 0.0001$; TgF344-AD treated compared to NTg: $P = 0.02$ and $P < 0.0001$, respectively; Fig. 4C and D). These results demonstrate that rescued hippocampal function contributes to rescue of pattern separation and executive function, and thus persistence of spatial memory deficits detected herein may correlate with pathology in neuronal network connected regions.

Tau pathology contributes to lack of spatial memory rescue

Tau pathology in TgF344-AD rats was assessed in the hippocampus and entorhinal cortex to determine potential contribution to observed behavioural phenotypes and treatment effects. To characterize tau pathology, we used antibodies that detected tau positive inclusions (Fig. 5 and Supplementary Fig. 6). PHF1 and CP13 are phosphorylation-specific antibodies that label the majority of pathological hyperphosphorylated tau, whereas MC1 is a conformational dependent antibody and preferentially labels pretangle neurons and paired helical filaments (Weaver *et al.*, 2000; Alonso *et al.*, 2018). The majority of PHF1+ inclusions clustered around amyloid-β plaques and morphologically resembled dystrophic neurites (Fig. 5A). A significant population of tau inclusions (~15–20%) were non-plaque associated [Fig. 5A(i)]. CP13 identified a similar pattern of tau-positive inclusions to PHF1 while MC1 labelling was sparse and preferentially labelled non-plaque associated inclusions (Supplementary Fig. 6).

We quantified PHF1+ plaque associated and non-plaque associated inclusions in the dentate gyrus and entorhinal cortex (Fig. 5 and Supplementary Fig. 7). Amyloid-β attenuation decreased plaque associated inclusions in the dentate gyrus ($P < 0.0001$), but had no effect on non-plaque associated inclusions ($P = 0.35$; Fig. 5B). Tau pathology exhibited a similar distribution in the entorhinal cortex [Fig. 5C and C(i)]. Importantly, there was no effect of treatment on either plaque associated ($P = 0.56$) or non-plaque associated inclusions ($P = 0.38$) in the entorhinal cortex (Fig. 5D), despite decreased amyloid-β coverage in treated compared to untreated TgF344-AD rats ($P = 0.004$; Fig. 5E). The regional differences in reduction of tau pathology may relate to differences in neuronal compromise/dysfunction in these regions, as a result of earlier establishment of pathologies in the entorhinal cortex in comparison to the hippocampus, which cannot be rescued by removal of amyloid-β alone. Thus, we quantified entorhinal cortical neuronal density and detected no overall effect of genotype and treatment on the number of neurons in the entorhinal cortex [$F(3,28) = 2.37$, $P = 0.09$; Fig. 5F]. Importantly, there was a significant effect in layer II entorhinal cortical neurons [$F(3,28) = 5.23$, $P = 0.005$; Fig. 5G]. Layer II entorhinal cortical neurons are involved in entorhinal

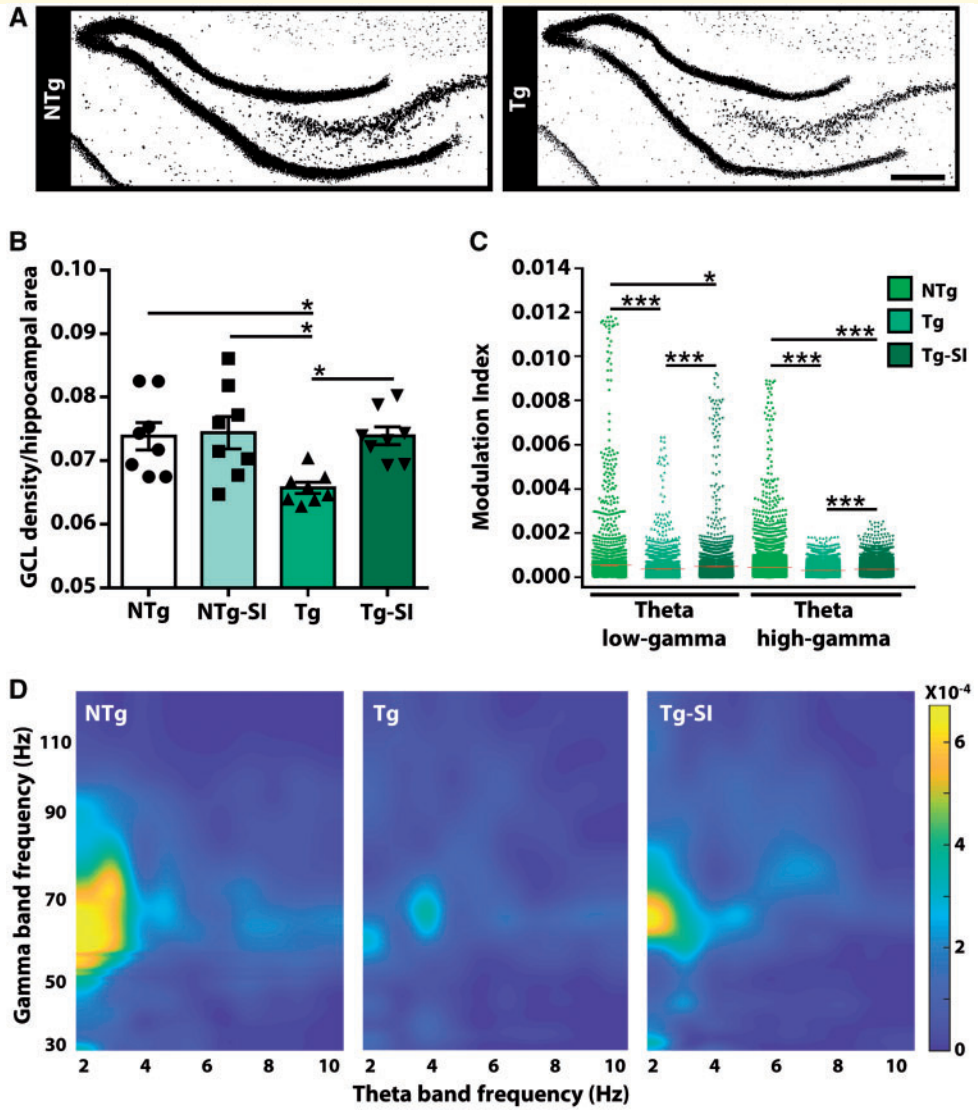

Figure 4 Rescue of hippocampal neuronal density and function in treated TgF344-AD rats. To determine if loss of hippocampal neurons and/or function contribute to the behavioural phenotypes, we determined neuronal density and cross-frequency coupling by *in vivo* electrophysiology. (**A**) Tg rats display a significant loss of NeuN (black) staining in the hippocampus, compared to NTg rats. Scale bar = 400 μm. (**B**) The density of NeuN staining in the granule cell layer (GCL) of Tg rats is significantly decreased by 11 ± 3.6 %, compared to NTgs, and is rescued by amyloid-β attenuation (n = 8). (**C**) TgF344-AD rats have impaired modulation between theta low-gamma and between theta high-gamma bands in the hippocampus, which are rescued by amyloid-β attenuation (NTg n = 8; Tg/Tg-SI n = 7). (**D**) 3D maps of phase amplitude coupling in the hippocampus (representative rat for each cohort) were generated by computing the modulation index as a measure of the coupling between the phase of the theta band with the amplitude of the gamma band. Modulation index values were encoded by colour and plotted according to theta and gamma frequency. 3D maps demonstrate a deficit in untreated Tg compared to NTg rats, and rescue by amyloid-β attenuation (mean ± SEM (indicated by a red line in **C**], one-way ANOVA with Holm-Sidak *post hoc* test (**B**), or with *t*-test with false discovery rate correction (**C**), $^{*}P < 0.05$; $^{***}P < 0.001$.

cortical-hippocampal circuitry, regulate spatial information, and represent the primary entorhinal cortical input into the dentate gyrus (Steward and Scoville, 1976; Hafting *et al.*, 2005; Ray *et al.*, 2014). Our findings that TgF344-AD rats exhibit significantly fewer neurons in layer II of the entorhinal cortex in comparison to NTg rats (P = 0.05) and a lack of treatment effect in both NTg and TgF344-AD rats (both P = 0.77) support the lack of rescue in spatial memory tasks.

Impaired entorhinal cortical-hippocampal connectivity persists after amyloid-β attenuation

In light of different effects of amyloid-β attenuation on tau pathology and neuronal loss in the hippocampus and entorhinal cortex, we conducted *in vivo* electrophysiological recordings to address functional outputs within the entorhinal cortex and its communication with the

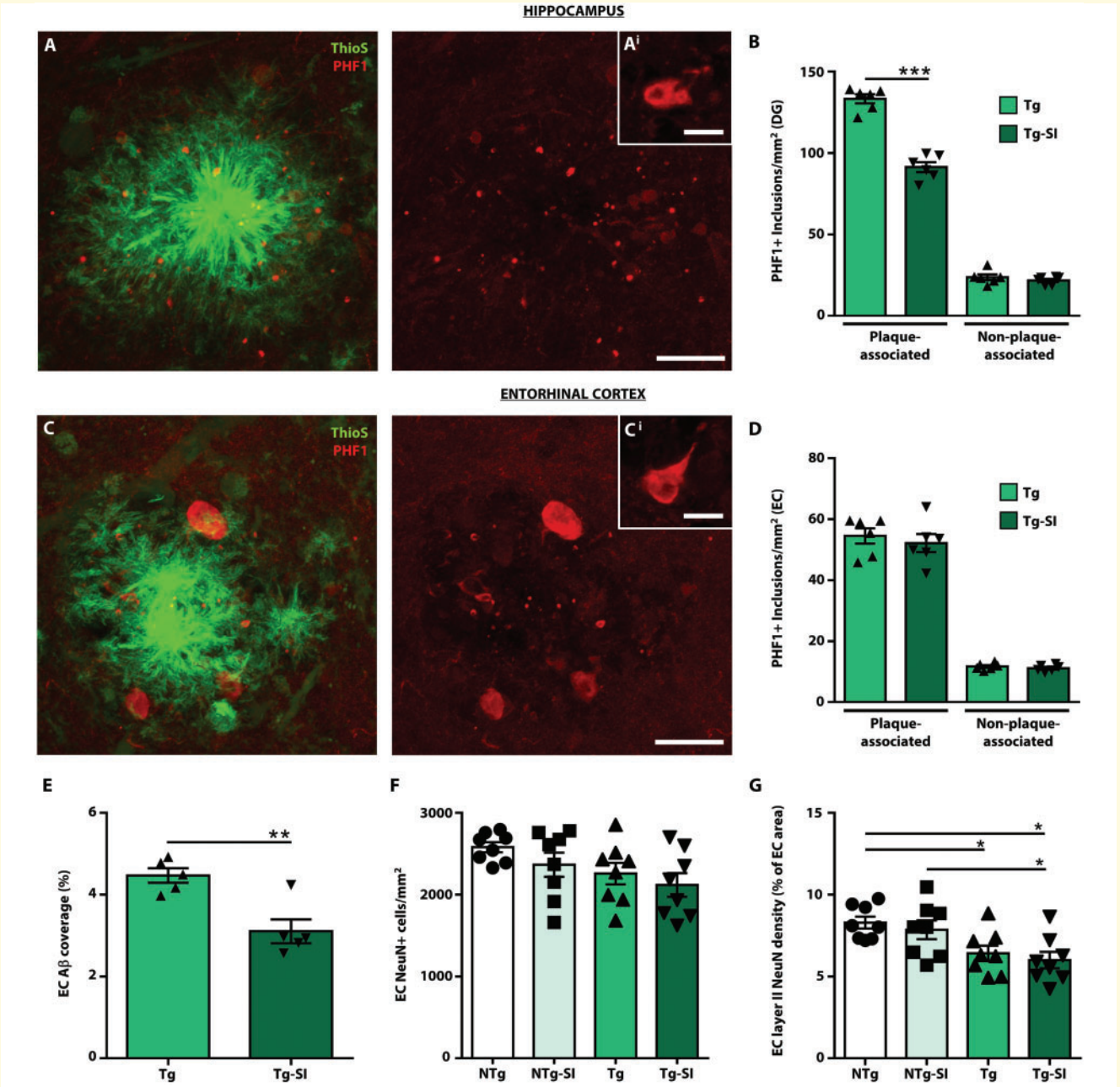

Figure 5 Amyloid-β attenuation decreases tau pathology in a brain region-dependent manner. Tau pathology was assessed in TgF344-AD rats (Tg, Tg-SI) by immunostaining with PHF1 to label hyperphosphorylated tau at S396/404 and Thioflavin-S (Thio-S) to label amyloid-β plaques. (**A**) PHF1+/Thio-S+ staining in the dentate gyrus (DG) of a Tg rat. Approximately 80–85% of PHF1+ inclusions (red) associate with amyloid-β plaques (green), representing dystrophic neurites. [**A**(**i**)] The remainder of the tau inclusions are non-plaque associated, representing pretangle inclusions. (**B**) PHF1+ inclusions were separated into plaque and non-plaque associated, and quantified by immunohistochemistry (Supplementary Fig. 7) in the dentate gyrus. Amyloid-β attenuation significantly decreased plaque-associated, but not non-plaque associated inclusions. [**C** and **C**(**i**)] PHF1+/Thio-S+ staining in the entorhinal cortex of a Tg rat indicating plaque-associated inclusions and non-plaque associated inclusions. (**D**) There was no effect of treatment on either plaque-associated or non-plaque associated inclusions in the entorhinal cortex (EC) (**E**), despite a reduction of amyloid-β plaques in the region. (**F**) No significant differences were detected in the number of total entorhinal cortical neurons across genotype and treatment (**G**); however, Tg and Tg-SI rats exhibit a decrease of neurons within layer II of the entorhinal cortex. Scale bars = 20 μm in **A** and **C**; 10 μm in **A**(**i**) and **C**(**i**). n = 6, mean ± SEM, two-sided unpaired t-test, $^{*}P < 0.05$; $^{**}P < 0.01$; $^{***}P < 0.001$.

hippocampus (Fig. 6). Electrodes were implanted in the right hippocampus and right medial entorhinal cortex of untreated and treated TgF344-AD and NTg rats. Spontaneous activity was amplified, recorded and analysed to examine cross-frequency coupling within the entorhinal cortex. Representative 3D maps of phase amplitude

coupling within the entorhinal cortex demonstrate a deficit in TgF344-AD rats, and a rescue by amyloid-β attenuation (Fig. 6A). An overall effect of genotype and treatment was detected on entorhinal cortical modulation index in theta low-gamma and theta high-gamma bands [$F(2,40191) = 113.00$, $P < 0.0001$; $F(2,81771) = 160.30$, $P < 0.0001$, respectively; Fig. 6B]. When compared to NTg rats, TgF344-AD rats exhibit deficits between theta low-gamma and between theta high-gamma bands, which are reversed by amyloid-β attenuation ($P < 0.0001$). Treated TgF344-AD rats exhibited a higher modulation index in both theta low-gamma and high-gamma bands when compared to NTg rats ($P < 0.0001$).

Critically, to assess network connectivity between entorhinal cortex and hippocampus, the entorhinal cortex was stimulated with one pulse at 500 mV and at 1000 mV (Supplementary Fig. 2). Regardless of treatment, TgF344-AD rats exhibited a decreased amplitude of hippocampal response (Fig. 6C). An overall effect was determined on response amplitude to 500 mV stimulation (Kruskal-Wallis chi-squared = 52.02, df = 2, $P < 0.0001$) and to 1000 mV stimulation (Kruskal-Wallis chi-squared = 35.04, df = 2, $P < 0.0001$; Fig. 6C). When compared to NTg rats, untreated and treated TgF344-AD rats have a significantly smaller hippocampal response to entorhinal cortical stimulation at 500 mV and 1000 mV ($P < 0.0001$; Fig. 6C and D). There was no effect of amyloid-β attenuation in TgF344-AD rats ($P = 0.17$ and $P = 0.18$, respectively). These data demonstrate that even though amyloid-β attenuation reverses neuronal dysfunction within hippocampal and within entorhinal cortical circuitry, the connectivity between these regions remains impaired. Neurodegeneration of these neuronal connections is exacerbated by accumulation of tau inclusions in the entorhinal cortex, and drives memory deficits even with the reduction of amyloid-β.

Discussion

A defining feature of Alzheimer's disease is progressive accumulation of amyloid-β and tau pathology that ultimately leads to defined patterns of cognitive decline with mild memory loss typically occurring first, followed by deficits in activities of daily living and executive function, and eventually dementia (Braak and Braak, 1991; Selkoe and Hardy, 2016). Our data support the hypothesis that removing amyloid-β pathology alone is not sufficient to completely clear tau pathology, and that tau pathology and neurodegeneration continue to accumulate, thereby providing a possible explanation for the cognitive deficits in patients in whom amyloid-β clearance has been effective. Supported by recent advances in understanding of tau pathology in Alzheimer's disease and preclinical models (Fu *et al.*, 2017, 2019; Busche *et al.*, 2019; Franzmeier *et al.*, 2019; Gordon *et al.*, 2019), we describe a potential mechanism for the successes in preclinical models and clinical failure of amyloid-β-targeted therapeutics.

In this report, we examined cognitive function in disease-bearing TgF344-AD rats with modest amyloid-β and tau pathology, and neuronal network dysfunction at study onset (Cohen *et al.*, 2013; Joo *et al.*, 2017; Bazzigaluppi *et al.*, 2018). To understand contributions of various pathologies to observed behavioural phenotype, we treated TgF344-AD rats with *scyllo*-inositol to lower amyloid-β, and sought to determine which aspects of cognition and pathology could or could not be rescued. The results reported herein are not due to off-target *scyllo*-inositol effects, as treatment did not alter brain *myo*-inositol nor incorporate into phosphatidylinositol family of lipids in rodents. Furthermore, *scyllo*-inositol had no direct effects on long-term potentiation measurements and no differences were detected in behaviour in treated or untreated NTg rats and mice (reviewed in Ma *et al.*, 2012).

With amyloid-β attenuation, we observed a rescue of deficits in pattern separation, as well as in latency to escape and search strategy used in the Barnes maze reversal task. Newborn neurons facilitate pattern separation and executive function (Lepousez *et al.*, 2015; Anacker and Hen, 2017; Toda *et al.*, 2018), and positively correlate with cognitive status in patients with mild cognitive impairment (Honer *et al.*, 2012; Tobin *et al.*, 2019). Our results indicated that TgF344-AD rats exhibit increased proliferation of hippocampal neural progenitor cells with deficits in neuronal differentiation, migration and survival. In support of our behavioural results, amyloid-β attenuation rescued neuronal maturation deficits while maintaining increased proliferation. In human Alzheimer's disease brains, maturation of newborn neurons is impaired (Moreno-Jiménez *et al.*, 2019). However, findings of increased (Jin *et al.*, 2004), unchanged (Boekhoorn *et al.*, 2006), and decreased proliferation were reported with disease progression (Crews *et al.*, 2010; Moreno-Jiménez *et al.*, 2019). Differential reports of proliferation between studies, both humans and rodents, may represent differences in disease progression, post-mortem delay and/or sensitivity of techniques used. While our study used repeated thymidine analogue treatments to label actively replicating cells and recently replicated cells, human studies are limited to immunohistochemical detection of markers each having inherent confounds to interpretation of cell population analysed.

We observed progressive hippocampal neuronal dysfunction in TgF344-AD rats due to large deficits in hippocampal cross-frequency coupling between theta to low-gamma and theta to high-gamma bands, compared to only theta to high-gamma impairments at 9 months of age (Bazzigaluppi *et al.*, 2018). Hippocampal function was rescued in TgF344-AD rats with amyloid-β attenuation, indicating both prevention of further decline and reversal of pre-existing deficits. The persistence of spatial memory deficits may thus be driven by tau pathology and/or deficits within

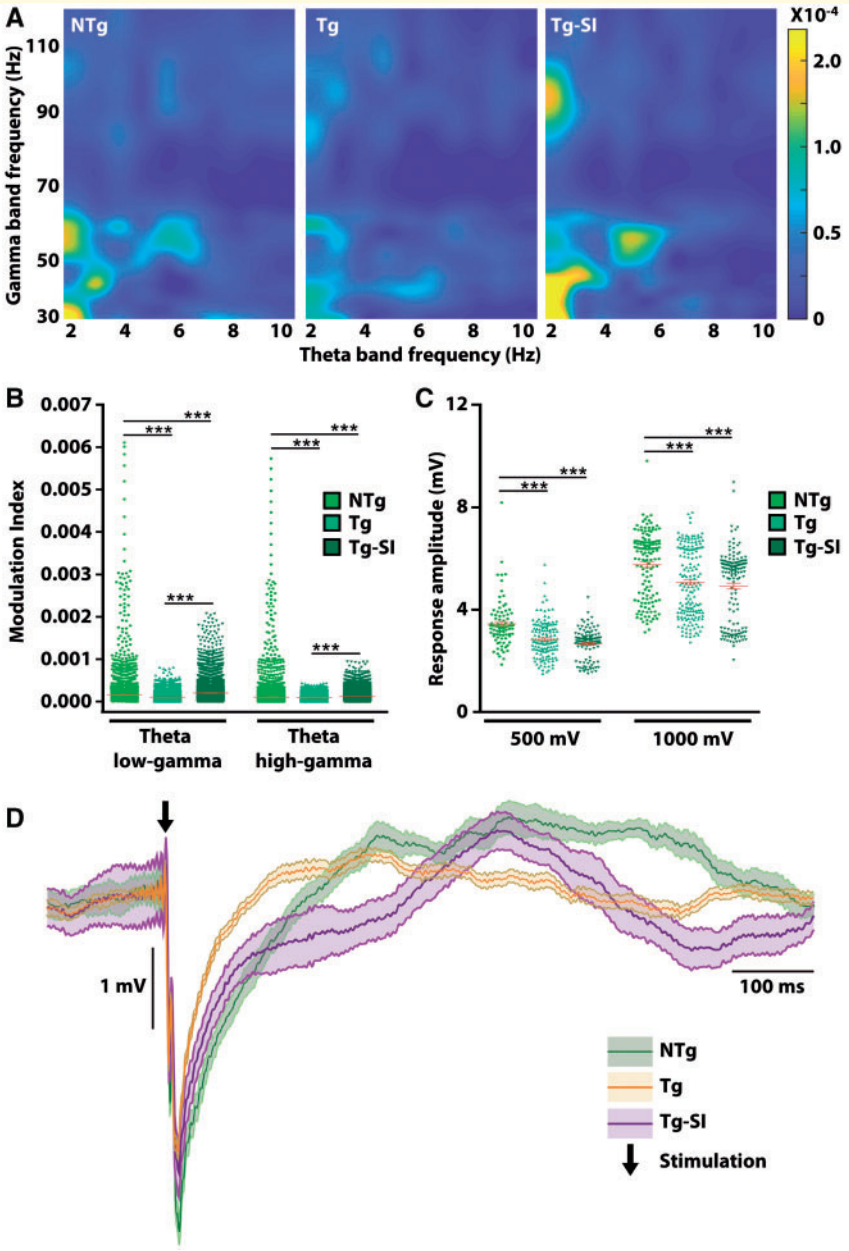

Figure 6 Impaired connectivity in entorhinal cortical-hippocampal circuit persists after amyloid-β attenuation. We assessed *in vivo* cross-frequency coupling in the entorhinal cortex, and connectivity with the hippocampus. (**A**) Representative 3D maps of phase amplitude coupling in the entorhinal cortex were generated by computing the modulation index as a measure of the coupling between the phase of the theta band with the amplitude of the gamma band. Modulation index values were encoded by colour and plotted according to theta and gamma frequency. 3D maps demonstrate a deficit in untreated Tg compared to NTg rats, and rescue by amyloid-β attenuation. (**B**) Modulation index of theta low-gamma and theta high-gamma bands in entorhinal cortex are impaired in Tg rats and rescued after treatment. To evaluate neuronal circuitry, we stimulated the entorhinal cortex and recorded hippocampal responses. (**C**) Tg rats, regardless of treatment, exhibit a significantly decreased hippocampal response to entorhinal cortical stimulation at 500 mV and 1000 mV, compared to NTg rats. (**D**) Representative neuronal trace demonstrating impaired hippocampal response to 500 mV entorhinal stimulation in Tg and Tg-SI rats. Black arrow indicates stimulation onset. NTg n = 8; Tg/Tg-SI n = 7. Red line indicates mean ± SEM, one-way ANOVA with t-test with false discovery rate correction (**B**) or a Kruskal-Wallis H test followed by Wilcoxon signed-rank test with false discovery rate correction (**C**). $^{***}P < 0.001$.

neuronal networks required for memory formation, specifically in the entorhinal cortex.

In preclinical Alzheimer's disease, tau propagates from the entorhinal cortex along functional neuronal connections, is facilitated by increasing amyloid-β load, and, with disease progression, associates with propagation of neurodegeneration and functional deficits (Braak and Braak, 1991; Ahmed *et al.*, 2014; Fu *et al.*, 2017; Jacobs

et al., 2018; Franzmeier *et al.*, 2019; Gordon *et al.*, 2019). Thus, our findings that amyloid-β attenuation significantly decreased plaque-associated tau inclusions in the dentate gyrus but not in the entorhinal cortex, and had no effect on non-plaque associated inclusions in either region, recapitulate previous findings after passive amyloid-β immunotherapy of 3xTg mice (Oddo *et al.*, 2004). It is important to note that in the TgF344-AD rats, physiological tau levels and subsequent pathology are the result of endogenous expression of rat tau.

Recent evidence indicates individual and synergistic effects of overexpression of tau and amyloid-β on neuronal function (Busche *et al.*, 2019). To understand if accumulation of tau pathology in the absence of amyloid-β accumulation contributes to neuronal dysfunction and thereby behaviour, we assessed *in situ* neuronal activity in the entorhinal cortex. TgF344-AD rats display strong deficits in modulation between theta to low-gamma and to high-gamma bands within the entorhinal cortex. We expected persistence of these deficits in treated rats, however, there was reversal with amyloid-β attenuation. In light of the data showing that overexpression of human mutant tau, P301L, in the mouse entorhinal cortex and the formation of tau inclusions lead to loss of excitatory neurons in the entorhinal cortex, disruption of regional grid cell function, and deficits in spatial memory (Fu *et al.*, 2017, 2019), we postulated that hypoconnectivity in entorhinal cortical-hippocampal circuitry may be driving spatial memory deficits, which we assessed by stimulating the entorhinal cortex with concurrent recordings in the hippocampus. We observed that both untreated and treated TgF344-AD rats have impaired hippocampal response to entorhinal cortical stimulation. Our results are in agreement with previous studies in TgF344-AD rats demonstrating synaptic signalling deficits in entorhinal cortical afferent synapses into the dentate gyrus at 6 months (Smith and McMahon, 2018), and progressive loss of functional connectivity measured by resting state functional MRI starting from 6 months (Anckaerts *et al.*, 2019).

We propose that in disease-bearing TgF344-AD rats after amyloid-β attenuation, the persistence of spatial memory deficits is driven by entorhinal cortical tau pathology and loss of layer II neurons leading to entorhinal cortical-hippocampal hypoconnectivity, whereas the rescue of pattern separation and executive function is driven by reduction in hippocampal tau pathology, improvements in hippocampal neurogenesis and neuronal function.

Although our results are limited by investigation of only one amyloid-β reducing treatment in a single model, anti-amyloid-β immunotherapies elicited similar outcomes in clinical trials to our study with *scyllo*-inositol. To date, most of the immunotherapy clinical trials have not shown efficacy in cognitive measures even though target engagement was evident. Similar to our study, immunotherapy trials for Alzheimer's disease demonstrated brain plaque clearance (Sevigny *et al.*, 2016; Ostrowitzki *et al.*, 2017; Nicoll *et al.*, 2019) or inhibition of further accumulation (Salloway *et al.*, 2018). In the case of AN-1792, extended clearance of amyloid plaques reduced aggregated tau in neuronal processes but not in cell bodies even 14 years post-active immunization (Boche *et al.*, 2010; Nicoll *et al.*, 2019). The changes in tau clearance after AN-1792 are similar to those we report in the hippocampus of *scyllo*-inositol treated TgF344-AD rats. Thus, our results contribute to the understanding of the lack of cognitive and tau pathological changes in active and passive immunotherapy trials in Alzheimer's disease patients.

Therefore, we have presented potential mechanisms to explain the failure of amyloid-β-targeted therapeutics to meet clinical cognitive endpoints. Even with strong target engagement and amyloid-β clearance, self-propagation of neurodegeneration and tau pathology may contribute to further cognitive decline. Our data support the necessity for discovering early biomarkers to accurately stage disease progression, and that the use of amyloid-β-targeted therapeutics may be more efficient in combinatorial treatment approaches.

Acknowledgements

The authors would like to thank Dr Peter Davies for his generous contribution of the PHF1, CP13 and MC1 antibodies, Drs Terrence Town and Tara M. Weitz for providing breeding pairs of TgF344-AD rats, and Dr Aaron Lai for technical support.

Funding

This work was supported by Canadian Institutes of Health Research MOP 142367 (J.M.) and PJT 156179 (B.S.), in part by the Canadian Consortium on Neurodegeneration in Aging, which was supported by a grant from the Canadian Institute of Health Research with funding from several partners, CAN-137794 (J.M., B.S.). This work was supported by an Ontario Graduate Scholarship (C.M.).

Competing interests

J.M. declares a potential competing interest as named inventor on patents related to *scyllo*-inositol. No other authors declare any competing interests.

Supplementary material

Supplementary material is available at *Brain* online.

References

Ahmed Z, Cooper J, Murray TK, Garn K, McNaughton E, Clarke H, et al. A novel in vivo model of tau propagation with rapid and progressive neurofibrillary tangle pathology: the pattern of spread

is determined by connectivity, not proximity. Acta Neuropathol 2014; 127: 667–83.
Alonso AD, Cohen LS, Corbo C, Morozova V, Elldrissi A, Phillips G, et al. Hyperphosphorylation of tau associates with changes in its function beyond microtubule stability. Front Cell Neurosci 2018; 12: 338.
Anacker C, Hen R. Adult hippocampal neurogenesis and cognitive flexibility–linking memory and mood. Nat Rev Neurosci 2017; 18: 335–46.
Anckaerts C, Blockx I, Summer P. Early functional connectivity deficits and progressive microstructural alterations in the TgF344-AD rat model of Alzheimer's disease: a longitudinal MRI study. Neurobiol Dis 2019; 124: 93–107.
Bazzigaluppi P, Beckett TL, Koletar MM, Lai AY, Joo IL, Brown ME, et al. Early-stage attenuation of phase-amplitude coupling in the hippocampus and medial prefrontal cortex in a transgenic rat model of Alzheimer's disease. J Neurochem 2018; 144: 669–79.
Benjamin Y, Hochberg Y. Controlling the false discovery rate: a practical and powerful approach to multiple testing. J R Stat Soc B 1995; 57: 289–300.
Boche D, Donald J, Love S, Harris S, Neal JW, Holmes C, et al. Reduction of aggregated Tau in neuronal processes but not in the cell bodies after Abeta42 immunisation in Alzheimer's disease. Acta Neuropathol 2010; 120: 13–20.
Boekhoorn K, Joels M, Lucassen PJ. Increased proliferation reflects glial and vascular-associated changes, but not neurogenesis in the presenile Alzheimer hippocampus. Neurobiol Dis 2006; 24: 1–14.
Bott JB, Muller MA, Jackson J, Aubert J, Cassel JC, Mathis C, et al. Spatial reference memory is associated with modulation of theta-gamma coupling in the Dentate Gyrus. Cereb Cortex 2016; 26: 3744–53.
Braak H, Braak E. Neuropathological stageing of Alzheimer-related changes. Acta Neuropathol 1991; 82: 239–59.
Busche MA, Wegmann S, Dujardin S, Commins C, Schiantarelli J, Klickstein N, et al. Tau impairs neural circuits, dominating amyloid-β effects, in Alzheimer models in vivo. Nat Neurosci 2019; 22: 57–64.
Canolty RT, Knight RT. The functional role of cross-frequency coupling. Trends Cogn Sci 2010; 14: 506–15.
Chrobak JJ, Buzsaki G. Gamma oscillations in the entorhinal cortex of the freely behaving rat. J Neurosci 1998; 18: 388–98.
Cohen RM, Rezai-Zadeh K, Weitz TM, Rentsendorj A, Gate D, Spivak I, et al. A transgenic Alzheimer rat with plaques, tau pathology, behavioral impairment, oligomeric Aβ and frank neuronal loss. J Neurosci 2013; 33: 6245–56.
Crews L, Adame A, Patrick C, Delaney A, Pham E, Rockenstein E, et al. Increased BMP6 levels in the brains of Alzheimer's disease patients and APP transgenic mice are accompanied by impaired neurogenesis. J Neurosci 2010; 30: 12252–62.
d'Abramo C, Acker CM, Jimenez HT, Davies P. Tau passive immunotherapy in mutant P301L mice: antibody affinity versus specificity. PLOS ONE 2013; 8: e62402.
Deacon RM. Burrowing: a sensitive behavioural assay, tested in five species of laboratory rodents. Behav Brain Res 2009; 200: 128–33.
Dorr A, Sahota B, Chinta LV, Brown ME, Lai AY, Ma K, et al. Amyloid-β-dependent compromise of microvascular structure and function in a model of Alzheimer's disease. Brain 2012; 135: 3039–50.
Fenili D, Brown M, Rappaport R, McLaurin J. Properties of *scyllo*-inositol as a therapeutic treatment of AD-like pathology. J Mol Med 2007; 85: 603–11.
Franzmeier N, Rubinski A, Neitzel J, Kim Y, Damm A, Na DL, et al. Functional connectivity associated with tau levels in ageing, Alzheimer's, and small vessel disease. Brain 2019; 142: 1093–107.
Fu H, Possenti A, Freer R, Nakano Y, Hernandez Villegas NC, Tang M, et al. A tau homeostasis signature is linked with the cellular and regional vulnerability of excitatory neurons to tau pathology. Nat Neurosci 2019; 22: 47–56.
Fu H, Rodriguez GA, Herman M, Emrani S, Nahmani E, Barrett G, et al. Tau pathology induces excitatory neuron loss, grid cell dysfunction and spatial memory deficits reminiscent of early Alzheimer's disease. Neuron 2017; 93: 533–41.
Gordon BA, Blazey TM, Christensen J, Dincer A, Flores S, Keefe S, et al. Tau PET in autosomal dominant Alzheimer's disease: relationship with cognition, dementia and other biomarkers. Brain 2019; 142: 1063–76.
Hafting T, Fyhn M, Molden S, Moser MB, Moser EI. Microstructure of a spatial map in the entorhinal cortex. Nature 2005; 436: 801–6.
Hawkes CA, Deng L, Fenili D, Nitz M, McLaurin J. In vivo uptake of β-amyloid by non-plaque associated microglia. Curr Alzheimer Res 2012; 9: 890–901.
Honer WG, Barr AM, Sawada K, Thornton AE, Morris MC, Leurgans SE, et al. Cognitive reserve, presynaptic proteins and dementia in the elderly. Transl Psychiatry 2012; 2: e114.
Illouz T, Madar R, Clague C, Griffioen KJ, Louzoun Y, Okun E. Unbiased classification of spatial strategies in the Barnes maze. Bioinformatics 2016; 32: 3314–20.
Jackson RJ, Rudinskiy N, Hermann AG, Croft S, Kim JM, Petrova V, et al. Human tau increases amyloid β plaque size but not amyloid β-mediated synapse loss in a novel mouse model of Alzheimer's disease. Eur J Neurosci 2016; 44: 3056–66.
Jacobs HIL, Hedden T, Schultz AP, Sepulcre J, Perea RD, Amariglio RE, et al. Structural tract alterations predict downstream tau accumulation in amyloid-positive older individuals. Nat Neurosci 2018; 21: 424–31.
Jessberger S, Clark RE, Broadbent NJ, Clemenson GD Jr, Consiglio A, Lie DC, et al. Dentate gyrus-specific knockdown of adult neurogenesis impairs spatial and object recognition memory in adult rats. Learn Mem 2009; 16: 147–54.
Jin K, Peel AL, Mao XO, Xie L, Cottrell BA, Henshall DC, et al. Increased hippocampal neurogenesis in Alzheimer's disease. Proc Natl Acad Sci U S A 2004; 101: 343–7.
Joo IL, Lai AY, Bazzigaluppi P, Koletar MM, Dorr A, Brown ME, et al. Early neurovascular dysfunction in a transgenic rat model of Alzheimer's disease. Sci Rep 2017; 7: 46427.
Lepousez G, Nissant A, Lledo PM. Adult neurogenesis and the future of the rejuvenating brain circuits. Neuron 2015; 86: 387–401.
Ma K, Thomason LAM, McLaurin J. *scyllo*-Inositol, preclinical, and clinical data for Alzheimer's disease. Adv Pharmacol 2012; 64: 177–212.
McLaurin J, Kierstead ME, Brown ME, Hawkes CA, Labremon MH, Phinney AL, et al. Cyclohexanhexol inhibitors of Abeta aggregation prevent and reverse Alzheimer phenotype in mouse model. Nat Med 2006; 12: 801–8.
Moreno-Jiménez EP, Flor-Garcia M, Toerreros-Roncal J, Rábano A, Cafini F, Pallas-Bazarra N, et al. Adult hippocampal neurogenesis is abundant in neurologically healthy subjects and drops sharply in patients with Alzheimer's disease. Nat Med 2019; 25: 554–60.
Morrone CD, Thomason LAM, Brown ME, Aubert I, McLaurin J. Effects of neurotrophic support and amyloid-targeted combined therapy on adult hippocampal neurogenesis in a transgenic model of Alzheimer's disease. PLOS ONE 2016; 11: e0165393.
Muñoz-Moreno E, Tudela R, López-Gil X, Soria G. Early brain connectivity alterations and cognitive impairment in a rat model of Alzheimer's disease. Alzheimer's Res Ther 2018; 10: 16.
Nicoll JAR, Nuckland GR, Harrison CH, Page A, Harris S, Love S, et al. Persistent neuropathological effects 14 years following amyloid-β immunization in Alzheimer's disease. Brain 2019; 142: 2113–26.
Oddo S, Billings L, Kesslak JP, Cribbs DH, LaFerla FM. Abeta immunotherapy leads to clearance of early, but not late, hyperphosphorylated tau aggregates via the proteasome. Neuron 2004; 43: 321–32.
Ostrowitzki S, Lasser RA, Dorflinger E, Scheltens P, Barkhof F, Nikolcheva T, et al. A phase III randomized trial of gantenerumab in prodromal Alzheimer's disease. Alzheimers Res Ther 2017; 9: 95.

Pettersen KH, Devor A, Ulbert I, Dale AM, Einevoll GT. Current-source density estimation based on inversion of electrostatic forward solution: effects of finite extent of neuronal activity and conductivity discontinuities. J Neurosci Methods 2006; 154: 116–33.

Ray S, Naumann R, Burgalossi A, Tang Q, Schmidt H, Brecht M. Grid-layout and theta-modulation of layer 2 pyramidal neurons in medial entorhinal cortex. Science 2014; 343: 891–6.

Rorabaugh JM, Chalermpalanupap T, Botz-Zapp CA, Fu VM, Lembeck NA, Cohen RM, et al. Chemogenetic locus coeruleus activation restores reversal learning in a rat model of Alzheimer's disease. Brain 2017; 140: 3023–38.

Salloway S, Honigberg LA, Cho W, Ward M, Friesenhahn M, Brunstein F, et al. Amyloid positron emission tomography and cerebrospinal fluid results from a crenezumab anti-amyloid-beta antibody double-blind, placebo-controlled, randomized phase II study in mild-to-moderate Alzheimer's disease (BLAZE). Alzheimers Res Ther 2018; 10: 96.

Selkoe DJ, Hardy J. The amyloid hypothesis of Alzheimer's disease at 25 years. EMBO Mol Med 2016; 8: 595–608.

Sevigny J, Chiao PL, Bussière T, Weinreb PH, Williams L, Maier M, et al. The antibody aducanumab reduces Aβ plaques in Alzheimer's disease. Nature 2016; 537: 50–6.

Smith LA, McMahon LL. Deficits in synaptic function occur at medial perforant path-dentate granule cell synapses prior to Schaffer collateral-CA1 pyramidal cell synapses in the novel TgF344-Alzheimer's Disease Rat Model. Neurobiol Dis 2018; 110: 166–79.

Squire LR, Wixted JT, Clark RE. Recognition memory and the medial temporal lobe: a new perspective. Nat Rev Neurosci 2007; 8: 872–83.

Steward O, Scoville SA. Cells of origin of entorhinal cortical afferents to the hippocampus and fascia dentata of the rat. J Comp Neurol 1976; 169: 347–70.

Stoiljkovic M, Kelley C, Stutz B, Horvath TL, Hajós M. Altered cortical and hippocampal excitability in TgF344-AD rats modeling Alzheimer's disease pathology. Cereb Cortex 2019; 29: 2716–27.

Tobin MK, Musaraca K, Disouky A, Shetti A, Bheri A, Honer WG, et al. Human hippocampal neurogenesis persists in aged adults and Alzheimer's disease patients. Cell Stem Cell 2019; 24: 974–82.

Toda T, Parylak SL, Linker SB, Gage FH. The role of adult hippocampal neurogenesis in brain health and disease. Mol Psychiatry 2018; 24: 67–87.

Tort AB, Komorowski WB, Manns JR, Kopell NJ, Eichenbaum H. Theta-gamma coupling increases during the learning of item-context associations. Proc Natl Acad Sci U S A 2009; 106: 20942–47.

Voorhees JR, Remy MT, Erickson CM, Dutca LM, Brat DJ, Pieper AA. Occupational-like organophosphate exposure disrupts microglia and accelerates deficits in a rat model of Alzheimer's disease. Aging Mech Dis 2019; 5: 3.

Weaver CL, Espinoza M, Kress Y, Davies P. Conformation change as one of the earliest alterations of tau in Alzheimer's disease. Neurobiol Aging 2000; 21: 719–27.